Volume 16
Number 12
28 March 2025
Pages 4903–5312

Chemical Science

rsc.li/chemical-science

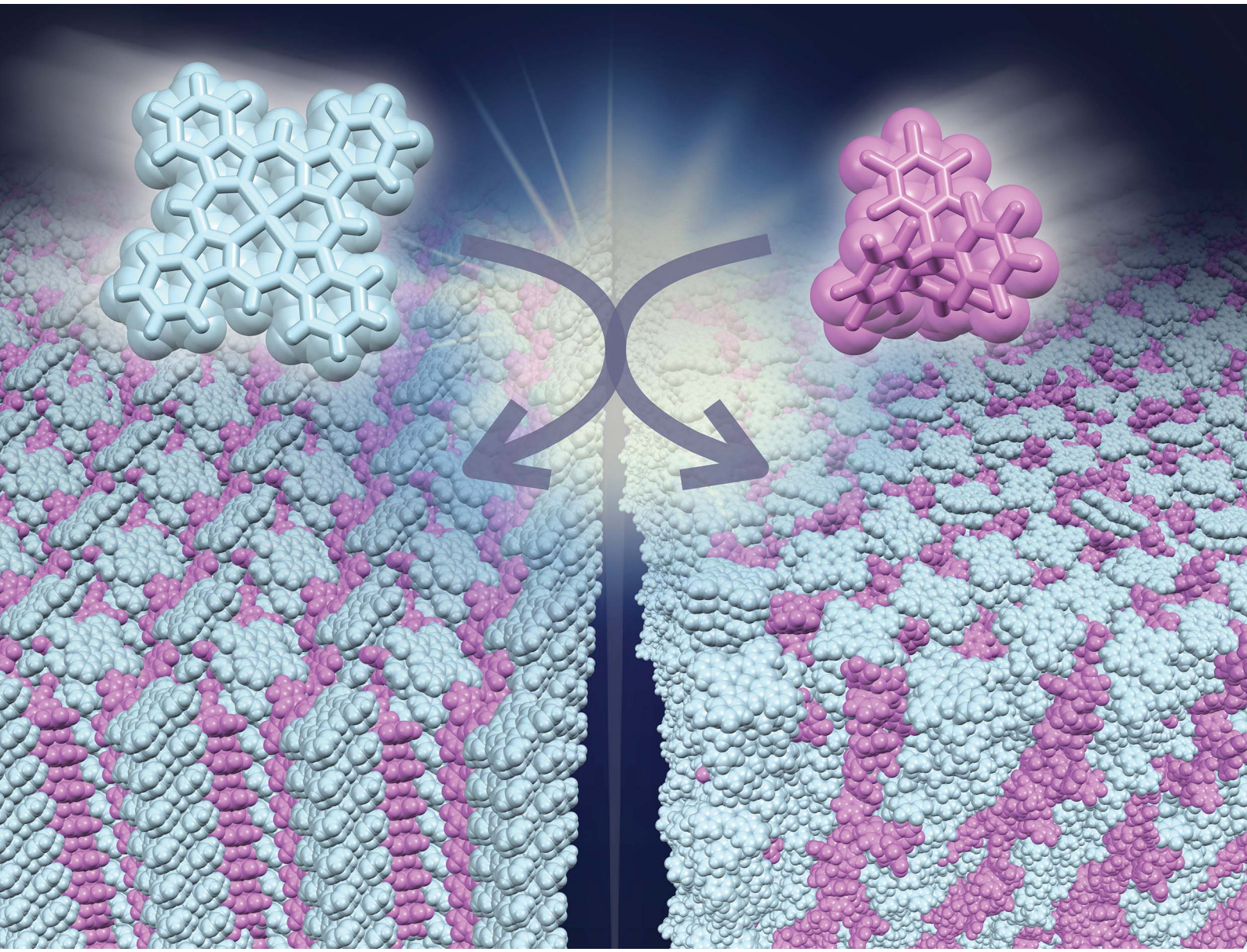

ISSN 2041-6539

ROYAL SOCIETY OF CHEMISTRY

EDGE ARTICLE
Hiromitsu Maeda *et al.*
Electrically conductive charge-segregated pseudo-polymorphs comprising highly planar expanded π-electronic cations

15 YEARS ANNIVERSARY

Chemical Science

ROYAL SOCIETY OF CHEMISTRY

EDGE ARTICLE

View Article Online
View Journal | View Issue

Cite this: *Chem. Sci.*, 2025, **16**, 4998

All publication charges for this article have been paid for by the Royal Society of Chemistry

Electrically conductive charge-segregated pseudo-polymorphs comprising highly planar expanded π-electronic cations†

Yohei Haketa, [a] Ryoya Nakajima,[a] Yuto Maruyama,[a] Hiroki Tanaka,[a] Wookjin Choi,[b] Shu Seki, [b] Shunsuke Sato, [c] Hitomi Baba,[c] Yoshiki Ishii, [d] Go Watanabe, [cd] Kirill Bulgarevich, [e] Kazuo Takimiya, [efg] Kenzo Deguchi,[h] Shinobu Ohki,[h] Kenjiro Hashi,[i] Takashi Nakanishi, [j] Yukihide Ishibashi, [k] Tsuyoshi Asahi,[k] Kazuchika Ohta [l] and Hiromitsu Maeda *[a]

Independently stacked positively and negatively charged π-electronic systems in charge-segregated columnar structures are desired for electronic properties derived from their electron-deficient and -rich assembling states, respectively. An expanded π-electronic cation, benzoporphyrin Au^{III} complex, was synthesized as the component of ion pairs in combination with counteranions. In contrast to benzoporphyrin, which is known for its insolubility in organic solvents, the ion pairs with bulky anions in this study are soluble in common organic solvents. The ion pairs formed charge-segregated assemblies as two pseudo-polymorphs of single-crystal and less-crystalline (LeC) states based on the stacking of the benzoporphyrin Au^{III} complex. XRD and solid-state NMR measurements, along with molecular dynamics (MD) simulation, revealed that the LeC states were formed by a less-ordered arrangement of constituting ions induced by bulky counteranions. The electric conductivity properties were observed in the single-crystal and LeC charge-segregated assemblies.

Received 8th November 2024
Accepted 6th February 2025

DOI: 10.1039/d4sc07576e

rsc.li/chemical-science

Introduction

The ordered arrangement of π-electronic systems is crucial for charge-carrier transport properties.[1] Expanded π-planes are adequate for achieving high performance in organic semiconductive materials.[1g] Since substituents affect the electronic states of molecules and their arrangement, π-electronic systems that have no substituents are in great demand.[1e] However, such systems have low solubility (high crystallinity), making it difficult to arrange the constituents to form assembled structures (Fig. 1a top left). A promising strategy is the preparation of ion pairs of charged π-electronic systems by combining them with counterions that improve solubility (Fig. 1a top right).[2] An appropriate combination of charged constituents enables facile handling of π-electronic systems to form counterion-dependent assemblies for applications (Fig. 1a bottom). In particular, independently stacked positively and negatively charged π-electronic systems are fascinating because of their ability to form electron-deficient and -rich assembling states, which can function as n- and p-type semiconductive pathways, respectively, in charge-segregated columnar structures.[3] Expanded π-systems contribute to influential dispersion forces that overcome electrostatic repulsion in charged columns. The potential positively charged π-systems are porphyrin Au^{III} complexes, which have been included in various ion-pairing assemblies in the form of crystals, supramolecular gels and liquid crystals

[a]*Department of Applied Chemistry, College of Life Sciences, Ritsumeikan University, Kusatsu 525-8577, Japan. E-mail: maedahir@ph.ritsumei.ac.jp*
[b]*Department of Molecular Engineering, Graduate School of Engineering, Kyoto University, Kyoto 615-8510, Japan*
[c]*Department of Physics, Graduate School of Science, Kitasato University, Sagamihara 252-0373, Japan*
[d]*Department of Data Science, School of Frontier Engineering, Kitasato University, Sagamihara 252-0373, Japan*
[e]*Center for Emergent Matter Science (CEMS), RIKEN, Wako 351-0198, Japan*
[f]*Department of Chemistry, Graduate School of Science, Tohoku University, Sendai 980-8578, Japan*
[g]*Advanced Institute for Materials Research (AIMR), Tohoku University, Sendai 980-8577, Japan*
[h]*Research Network and Facility Services Division, National Institute for Materials Science (NIMS), Tsukuba 305-0003, Japan*
[i]*Center for Basic Research on Materials, National Institute for Materials Science (NIMS), Tsukuba 305-0003, Japan*
[j]*Research Center for Materials Nanoarchitectonics (MANA), National Institute for Materials Science (NIMS), Tsukuba 305-0044, Japan*
[k]*Department of Applied Chemistry, Graduate School of Science and Engineering, Ehime University, Matsuyama 790-8577, Japan*
[l]*Interdisciplinary Graduate School of Science and Technology, Shinshu University, Ueda 386-8567, Japan*

† Electronic supplementary information (ESI) available: Synthetic procedures, analytical data, computational details and CIF files for the single-crystal X-ray structural analysis. CCDC 2387040–2387044. For ESI and crystallographic data in CIF or other electronic format see DOI: https://doi.org/10.1039/d4sc07576e

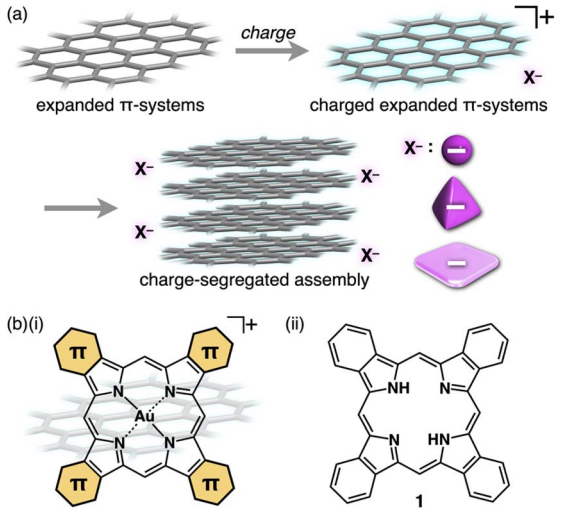

Fig. 1 (a) Expanded π-electronic systems that have no peripheral substituents (top left) and their charged and ion-pairing states (top right, represented as cations), forming a charge-segregated assembly by stacking (bottom) and (b) (i) π-expanded porphyrin Au^{III} complexes as expanded π-electronic cations that can be used in (a) and (ii) benzoporphyrin **1**. The positive signs were omitted in the charge-segregated assembly in (a).

depending on the substituents.[4,5] Expansion of π-electronic systems can be achieved by modifications at the pyrrole β-positions (Fig. 1b(i)). Numerous porphyrin derivatives that have been synthesized to date offered the choice to use benzoporphyrin[6] **1** (Fig. 1b(ii)) as a framework to provide highly planar charged expanded π-electronic systems. Large planes of benzoporphyrin-based cations are suitable for stacking to form charge-segregated assemblies, whose packing structures can be controlled by coexisting counteranions. The arrangement of substituent-free planar cations and bulky anions can be modulated by crystallization conditions. This study shows π-expanded cation-based ion-pairing assemblies in single-crystal and pseudo-polymorph less-crystalline (LeC) states and their electric conductivity properties derived from the charge-segregated assemblies.

Results and discussion

Synthesis and characterization of expanded π-electronic cations

Benzoporphyrins, including metal complexes, can be synthesized from bicyclo[2.2.2]octadiene precursors *via* retro-Diels–Alder reactions.[6f] In this study, Au^{III} complexation was conducted for bicycloporphyrin **2** to afford the Au^{III} complex **2au**$^+$ mainly as a triflate (OTf^-) ion pair by treatment with $KAuCl_4$ in the presence of AgOTf and NaOAc (Fig. 2 top). The ion pair **2au**$^+$-OTf^- was converted to the Cl^- ion pair **2au**$^+$-Cl^- in 28% yield (two steps) using an ion-exchange resin (Amberlite: IRA402BL Cl). As the selection of the counteranions was crucial in this study, the ion-pair metathesis of **2au**$^+$-Cl^- with $AgPF_6$, $LiB(C_6F_5)_4$ (LiFABA), $NaB(3,5\text{-}(CF_3)_2C_6H_3)_4$ (NaBArF) and NaPCCp (PCCp$^-$: pentacyanocyclopentadienide)[7] afforded the

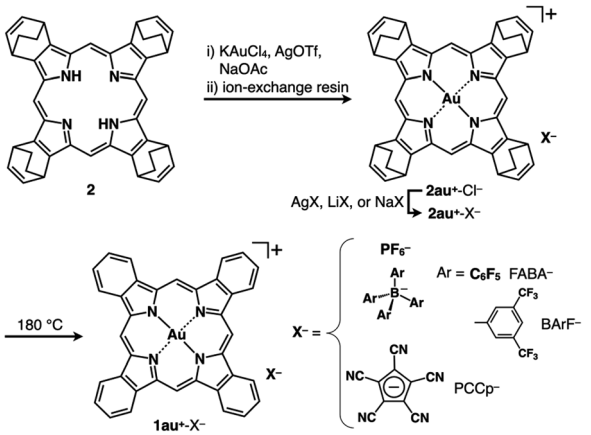

Fig. 2 Synthesis of benzoporphyrin Au^{III} complex ion pairs **1au**$^+$-X^- ($X^- = PF_6^-$, $FABA^-$, $BArF^-$ and $PCCp^-$) *via* the corresponding bicycloporphyrin Au^{III} complex ion pairs **2au**$^+$-X^-.

corresponding ion pairs **2au**$^+$-X^- ($X^- = PF_6^-$, $FABA^-$, $BArF^-$ and $PCCp^-$) in 66–76% yields. The obtained ion pairs were characterized by ^1H, ^{13}C and ^{19}F NMR and ESI-TOF-MS. DMSO solutions of **2au**$^+$ ion pairs (4 μM) exhibited Soret and Q-bands at 392 and 507/542 nm, respectively, indicating that **2au**$^+$ exists as a monomeric state with a negligible counteranion effect on the electronic properties of **2au**$^+$ (Fig. S12†).[8] **2au**$^+$-$FABA^-$ and **2au**$^+$-$BArF^-$ were also characterized by X-ray analysis for single crystals prepared by vapour diffusion from CH_3CN/water (Fig. 3, S18 and S19†). In the solid-state structures, the cation **2au**$^+$, refined as one of the stereoisomers, formed stacked dimers with stacking/Au···Au distances of 3.56/3.41 and 3.48/3.37 Å, respectively, and a rotation of ~45° owing to dispersion forces

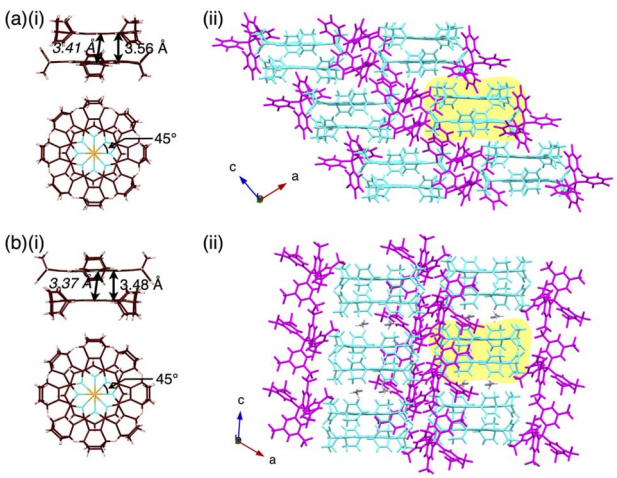

Fig. 3 Single-crystal X-ray structures of (a) **2au**$^+$-$FABA^-$ and (b) **2au**$^+$-$BArF^-$: (i) side and top views of stacked dimers with stacking and Au···Au (italic) distances and (ii) packing structures with the yellow parts corresponding to the stacked dimers in (i). Atom colour codes in (i): brown, pink, blue and orange refer to carbon, hydrogen, nitrogen and gold, respectively. Colour codes in (ii): cyan and magenta refer to cation and anion parts, respectively. Solvent molecules are omitted in (a), whereas CH_3CN molecules are shown in (b).

at the core planes and β-bicyclo units (Fig. 3a and b(i)). The stacking of **2au**$^+$ is visualized by Hirshfeld surface analysis, which shows a bow-tie arrangement of red and blue triangles in the shape-index property and flat regions in the curvedness property (Fig. S24 and S25†).[9] Mean-plane deviations of 0.052/0.068 and 0.036 Å for stacking **2au**$^+$ planes (core 25 atoms), respectively, indicate slightly curved **2au**$^+$ planes, owing to the Au···Au distances being less than the stacking distances. Such remarkably close Au···Au distances are also ascribable to the orbital interactions arising from overlap of the $5d_{z^2}$ and $6p_z$ orbitals of the adjacent Au^{III}.[10] The stacked **2au**$^+$ dimers in ion pairs are aligned along the *c*-axis with an offset, which is smaller in **2au**$^+$-BArF$^-$ with a longer distance between the stacked dimers by including two CH_3CN molecules (Fig. 3a and b(ii)). In either case, counteranions are located at the side of the stacked **2au**$^+$ dimers. In particular, BArF$^-$ anions are located proximally at the side of the stacked **2au**$^+$ dimers, forming a pseudohexagonally arranged packing structure along the *c*-axis (Fig. S19a†).

Stacking of **2au**$^+$ by overcoming electrostatic repulsion was also observed in the solution state. In CD_3CN, the ^{1}H NMR of **2au**$^+$-FABA$^-$ showed broad signals at 9.96, 8.37/6.94, 5.98 and 3.49–1.30 ppm ascribable to *meso*-CH, bicyclo-sp^2-CH, bicyclo-bridged methine-CH and bicyclo-sp^3-CH, respectively, for the stacked dimer.[11] Concentration-dependent UV/vis absorption spectra of **2au**$^+$-FABA$^-$ in CH_3CN exhibited a blue shift of λ_{max} from 389 to 374 nm when increasing the concentration from 1.0×10^{-6} to 1.0×10^{-5} M, suggesting the formation of an H-like stacked dimer at the higher concentration (Fig. S71†). The transition dipole moments of **2au**$^+$ in the optimized structure of the stacked dimer **2au**$^+_2$ based on PCM-GD3BJ-B3LYP/6-31+G(d,p) with LanL2DZ for Au (CH_3CN) are arranged at ∼45°, suggesting that the H-like stacking mode induces a blue shift (Fig. S61a†).[12] In addition, TD-DFT calculation of the optimized **2au**$^+_2$ revealed an absorption at 375 nm, which is blue-shifted by 16 nm compared to the monomer state (Fig. S46†).

According to the synthetic procedure for benzoporphyrin **1**,[6f] **2au**$^+$-X$^-$ (X$^-$ = PF_6^-, FABA$^-$, BArF$^-$ and PCCp$^-$) were quantitatively transformed to the corresponding benzoporphyrin ion pairs **1au**$^+$-X$^-$ by heating at 180 °C for 20–60 min in the absence of solvent (Fig. 2 bottom). In contrast to **1**,[6f] which is insoluble in most organic solvents, the obtained **1au**$^+$-X$^-$ showed enhanced solubility. For example, **1au**$^+$-FABA$^-$ was soluble in acetone, DMF, CH_3CN and DMSO. In contrast, another ion pair **1au**$^+$-Cl$^-$, which was synthesized from **2au**$^+$-Cl$^-$, was not soluble in these solvents.[13] It is noteworthy that **1au**$^+$ is soluble with facile handling in the form of the ion pairs with appropriate counteranions, although the optimized structure of **1au**$^+$ estimated at B3LYP/6-31+G(d,p) with LanL2DZ for Au[12] exhibits completely planar geometry with a mean-plane deviation of 0.00 Å (Fig. S29†). ^{1}H NMR of **1au**$^+$-FABA$^-$ in DMSO-d_6 (1.0 mM), as an example, at r.t. exhibited broad signals at 10.21, 9.18 and 8.11 ppm, suggesting soluble but aggregated structures as also indicated by concentration-dependent ^{1}H NMR (Fig. S74†).[14] Such ^{1}H NMR signals in the downfield region suggested the aromatic ring current effect of **1au**$^+$, which was further supported by nucleus-independent chemical shift (NICS) and the anisotropy of the current induced density (ACID) calculations (Fig. S54 and S55†). Interestingly, ^{19}F NMR in the same solvent shows sharp signals derived from FABA$^-$ in the dispersed state. The UV/vis absorption spectrum of **1au**$^+$-FABA$^-$ in DMSO (4 μM), as a monomer state, exhibits Soret and Q bands of 408 and 564/616 nm, respectively (Fig. 4a), which are more red-shifted than those of **2au**$^+$-FABA$^-$. The TD-DFT-based UV/vis absorption stick spectrum of **1au**$^+$ in DMSO shows that these absorptions are mainly derived from the HOMO−1-to-LUMO+1 and HOMO-to-LUMO+1 transitions, respectively (Fig. 4a inset, S49†).

The ^{1}H NMR of **1au**$^+$-FABA$^-$ in CD_3CN (1.0 mM) shows broader signals than those in DMSO-d_6, suggesting more aggregated structures in the less polar solvent (Fig. S9†). Similar to **2au**$^+$-FABA$^-$, **1au**$^+$-FABA$^-$ shows a λ_{max} blue-shift from 402 to 384 nm upon increasing the concentration from 1.8×10^{-7} to 2.0×10^{-5} M in CH_3CN, suggesting the formation of H-like stacked structures (Fig. 4b(i) and S72†). Such a blue shift of the λ_{max} is also observed in variable-temperature (VT)-UV/vis absorption spectra at lower temperatures (Fig. 4b(ii)). TD-DFT calculation of the optimized structure for the stacked dimer **1au**$^+_2$ at PCM-B3LYP-GD3BJ/6-31+G(d,p) with LanL2DZ for Au (CH_3CN) suggests a slightly blue-shifted Soret band compared to that of the monomeric state (Fig. S51†). The dimerization constant (K_{dim}) of **1au**$^+$ for **1au**$^+$-FABA$^-$ is estimated to be 5 ×

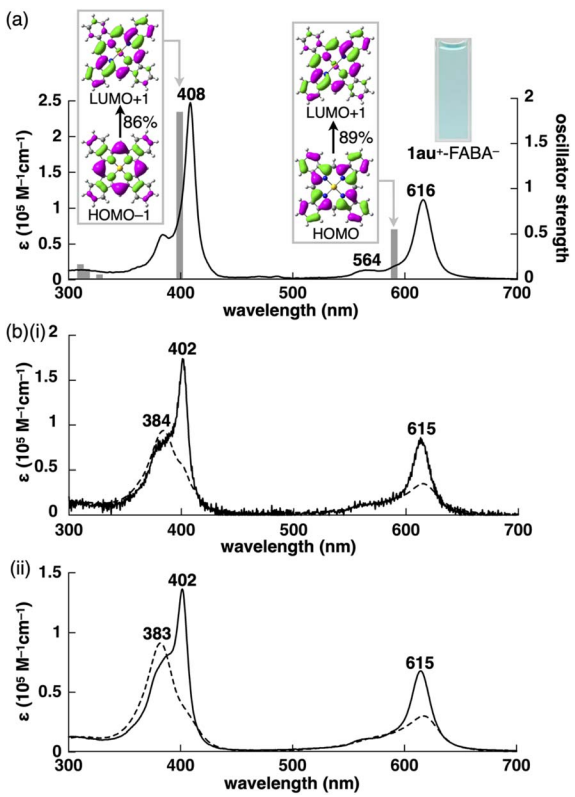

Fig. 4 (a) UV/vis absorption spectrum of **1au**$^+$-FABA$^-$ in DMSO (4 μM) (inset: photograph of the DMSO solution (4 μM)) and TD-DFT-based UV/vis absorption stick spectrum (grey bar) of **1au**$^+$ at PCM-B3LYP-GD3BJ/6-31+G(d,p) with LanL2DZ for Au (DMSO) and (b) UV/vis absorption spectra of **1au**$^+$-FABA$^-$ in CH_3CN according to (i) concentrations (solid line: 0.18 μM and broken line: 20 μM) and (ii) temperatures (solid line: 70 °C and broken line: −40 °C).

10^6 M^{-1} in CH_3CN at r.t. from concentration-dependent UV/vis absorption spectral changes (Fig. S72†). π-Expansion of positively charged π-electronic systems induces influential dispersion forces, which enable the stacking of identically charged π-electronic systems.

Single-crystal-state charge-segregated assemblies

Prism-shaped single crystals of the ion pairs **1au**$^+$-X^- (X^- = $FABA^-$, $BArF^-$ and $PCCp^-$), obtained from $CH_3CN/CHCl_3$,[15] 1,1,1-trichloroethane/*n*-heptane and DMF/*o*-dichlorobenzene, respectively, were suitable for X-ray analysis, revealing the exact structures of the ion pairs and their assembled structures (Fig. 5). In these structures, the cation **1au**$^+$, showing planar geometry with mean-plane deviations (core 25 atoms) of 0.016, 0.031/0.011 and 0.023 Å, respectively, forms closely stacked columnar structures with stacking distances of 3.29, 3.36/3.44 and 3.37 Å, respectively, in the charge-segregated mode (Fig. 5a–c(i)). The stacked parts of **1au**$^+$ are clearly shown by Hirshfeld surface analysis, exhibiting a bow-tie arrangement of red and blue triangles in the shape-index property and flat regions in the curvedness property (Fig. S26–S28†).[9] The Au···Au distances are 4.76, 3.93/4.59 and 3.81 Å, respectively, suggesting that the offset stacking of the cations is larger for **1au**$^+$-$FABA^-$. The angles of 44.1°, 48.4°/60.1° and 62.1° are estimated, respectively, for the lines passing through two Au atoms of stacked **1au**$^+$ to the corresponding 41-atom mean planes. In these ion pairs, counteranions $FABA^-$, $BArF^-$ and $PCCp^-$ are located at the side of the columnar structures (Fig. 5a–c(ii) and (iii)). The ion-pair crystals **1au**$^+$-$FABA^-$, **1au**$^+$-$BArF^-$ and **1au**$^+$-$PCCp^-$ formed orthorhombic, monoclinic and orthorhombic packing, respectively, with the columns of stacked **1au**$^+$ aligned along the *a*-, *c*- and *a*-axes, respectively, which are the long axes of the prism crystals (Fig. S23†). Notably, the stacked **1au**$^+$ in the columns are tilted, with angles of 30.4°, 2.9°/3.0° and 21.2°, respectively, relative to the stacking axis (Fig. 5a–c(ii)). Interestingly, in the crystal packing of **1au**$^+$-$FABA^-$, an ion-pair framework composed of columnar cation structures and counteranions forms two tubular spaces per unit cell, with a volume of 5.56 nm^3, containing disordered solvent molecules. The solvent molecules in the single crystal are not removed after heating at 100 °C under vacuum, as revealed by the X-ray analysis.

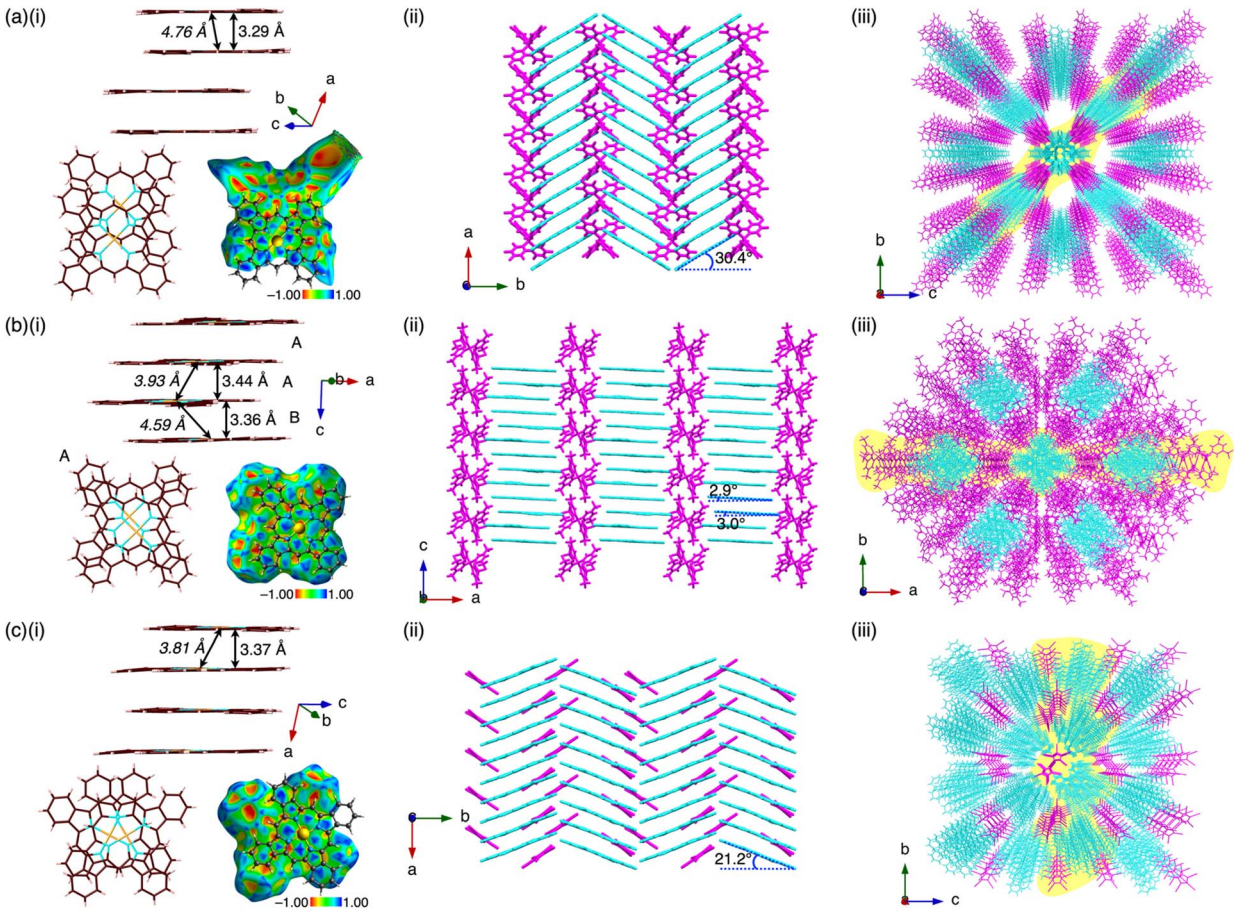

Fig. 5 Single-crystal X-ray structures of (a) **1au**$^+$-$FABA^-$, (b) **1au**$^+$-$BArF^-$ and (c) **1au**$^+$-$PCCp^-$: (i) side views of the columnar structures of stacked **1au**$^+$ with stacking and Au···Au (italic) distances and top views along with Hirshfeld surface mapped over the shape-index property of the stacked dimer, (ii) packing structures of columns of stacked **1au**$^+$ and counteranions and (iii) packing structures with the yellow parts corresponding to the packing structures in (ii). In (b), the different types of stacking arrangements are indicated by A and B (stacking arrangement A is shown as a representative). Atom colour codes in (i): brown, pink, blue and orange refer to carbon, hydrogen, nitrogen and gold, respectively. Colour codes in (ii and iii): cyan and magenta refer to cation and anion parts, respectively.

To evaluate the stacking behaviour of **1au**$^+$ in the crystal structures, energy decomposition analysis (EDA)[16,17] was performed using the fragment molecular orbital (FMO) method (FMO2-MP2) with mixed basis sets including NOSeC-V-DZP with MCP with NOSeC-V-TZP with MCP for Au.[18,19] The EDA calculations using FMO yielded E_{es}, E_{disp}, E_{ct} and E_{ex} (energies for electrostatic, dispersion, charge-transfer forces and exchange repulsion, respectively) and E_{tot} (total energy). In the columnar structure of **1au**$^+$ in **1au**$^+$-FABA$^-$, an E_{tot} of −164.2 kcal mol^{-1} is observed, whereas E_{disp} and E_{es} are −214.0 and 6.5 kcal mol^{-1}, respectively, indicating that E_{disp} is a major force in the stacking structure (Fig. 6 and S58†). EDA calculations for **1au**$^+$-BArF$^-$ and **1au**$^+$-PCCp$^-$ also elucidated similar energy balances for neighbouring π-electronic ions (Fig. S59 and S60†).

Crystal-state absorptions of the ion pairs **1au**$^+$-FABA$^-$, **1au**$^+$-BArF$^-$ and **1au**$^+$-PCCp$^-$ were evaluated *via* optical microscopy for spectroscopic examination (Fig. S75 and S76†). In **1au**$^+$-FABA$^-$, the absorptions at 587 and 623 nm, which are slightly blue- and red-shifted, respectively, compared to those of the monomer in DMSO (616 nm), are ascribable to the exciton coupling in a predominantly J-like arrangement and also very weak coupling for orthogonally arranged transition dipole moments (Fig. 7 and S62†). These behaviours are derived from the D_{4h} geometry of **1au**$^+$. Similar to **1au**$^+$-FABA$^-$, the crystal-state absorption of **1au**$^+$-PCCp$^-$ shows absorptions at 588 and 623 nm, which are ascribable to the exciton coupling of stacked **1au**$^+$. On the other hand, **1au**$^+$-BArF$^-$ mainly exhibits a blue-shifted broad absorption at 585 nm with a shoulder at 654 nm. The blue-shifted absorption can be attributed to the larger contribution of the H-like arrangement of transition dipoles in the stacked **1au**$^+$ (Fig. S62†).

Charge-segregated assemblies of π-electronic ion pairs show fascinating electric conductivity properties. The electric conductivity properties of stacked **1au**$^+$ in the ion pairs (**1au**$^+$-FABA$^-$, **1au**$^+$-BArF$^-$ and **1au**$^+$-PCCp$^-$) were evaluated by flash-photolysis time-resolved microwave conductivity (FP-TRMC) measurements (Fig. 8a and S91†).[20] Electric conductivity ($\phi\Sigma\mu$) values of 4.6×10^{-9}, 9.2×10^{-9} and 2.9×10^{-9} m^2 V^{-1} s^{-1} were

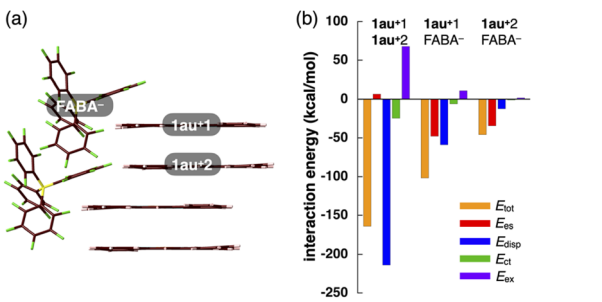

Fig. 6 Decomposition of the total intermolecular interaction energies (E_{tot}) of **1au**$^+$-FABA$^-$ for (a) the single-crystal X-ray structure and (b) estimated interaction energies (kcal mol^{-1}) according to EDA based on the FMO2-MP2 method using a basis set of NOSeC-V-DZP with MCP with NOSeC-V-TZP with MCP for Au (see Table S4† for the complete data list). Colour codes in (i): brown, pink, blue, yellow, green and orange refer to carbon, hydrogen, nitrogen, boron, fluorine and gold, respectively.

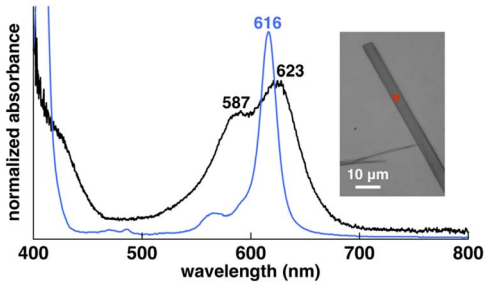

Fig. 7 Solid-state UV/vis absorption spectra of **1au**$^+$-FABA$^-$ in the single crystal (black line) and in DMSO (4 μM) (blue line) as a reference (inset: photograph of the single crystal (red circle indicates the position of measurement)).

observed for the longer axes of the respective single crystals. Clear anisotropic electric conductivity was shown in **1au**$^+$-BArF$^-$ (7.9×10^{-9} m^2 V^{-1} s^{-1} for the shorter axis). These values are comparable to and greater than those of previously reported charge-segregated assemblies.[3] The order of the $\phi\Sigma\mu$ values, **1au**$^+$-BArF$^-$ > **1au**$^+$-FABA$^-$ > **1au**$^+$-PCCp$^-$, is consistent with the theoretically estimated transfer integrals t at PW91/TZP for the stacked **1au**$^+$ units in the crystal structures, showing hole transfer integrals $|t|_h$ of 118.5/50.5, 21.3 and 9.8 meV, respectively (Fig. 8b and S63†).[21] Furthermore, theoretically estimated HOMO band dispersions using the tight-binding approximation[22] for the stacked **1au**$^+$ in the single-crystal structures of **1au**$^+$-FABA$^-$, **1au**$^+$-BArF$^-$ and **1au**$^+$-PCCp$^-$ exhibited one-dimensional band structures, which are consistent with the stacking structures of **1au**$^+$ (Fig. S64†). The Fermi levels lie in the middle of the band gaps, suggesting that charge-segregated assemblies comprising stacked **1au**$^+$ exhibit semiconductive behaviours. In the discussed ion pairs, decreased on-site Coulomb repulsion between stacked π-electronic cations with expanded π-electronic systems would induce hole transport rather than electron transport. The conductivity transients

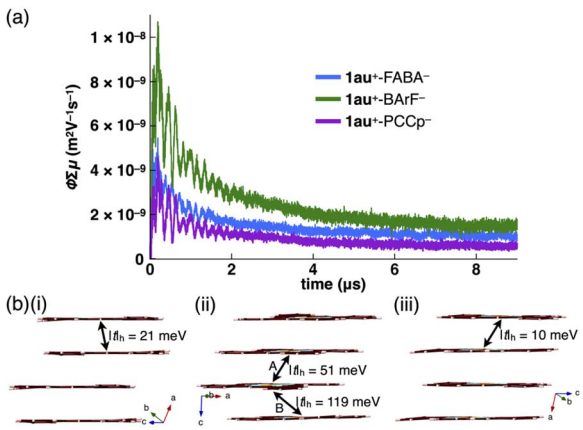

Fig. 8 (a) Photoconductivity transients observed upon excitation at 355 nm, 9.1×10^{15} photons per cm^2 per pulse, for the long axis of the single crystals of **1au**$^+$-FABA$^-$ (blue), **1au**$^+$-BArF$^-$ (green) and **1au**$^+$-PCCp$^-$ (purple) and (b) stacked **1au**$^+$ in the single crystal structures of (i) **1au**$^+$-FABA$^-$, (ii) **1au**$^+$-BArF$^-$ and (iii) **1au**$^+$-PCCp$^-$ and hole transfer integrals ($|t|_h$) estimated at PW91/TZP. Stacking modes A and B in (ii) correspond to Fig. 5b(i).

recorded under an SF_6 atmosphere with negligible quenching of charge carriers suggest a major contribution from holes photo-injected into the assemblies (Fig. S92†).[23]

Charge-segregated assemblies in pseudo-polymorph less-crystalline states

Substituent-free benzoporphyrins in the forms of free base and metal complexes have been known to show highly crystalline states after heating the corresponding bicyclo[2.2.2]octadiene precursors in the film state.[6h] In contrast, **1au**$^+$ as ion pairs can form bulk materials that are not single crystals *via* recrystallization from appropriate solvents. Precipitation of **1au**$^+$-FABA$^-$ from acetone/*n*-hexane provided a material (labelled as **1au**$^+$-FABA^-_P) that appeared to differ from the single crystals (Fig. 9a inset).[24] The synchrotron XRD of **1au**$^+$-FABA^-_P at 25 °C exhibited broad peaks instead of crystalline diffraction, suggesting the formation of an LeC state for the obtained precipitates. The diffraction peaks of 1.81, 1.04, 0.90, 0.68, 0.60, 0.52, 0.50, 0.45, 0.41 and 0.34 nm, showing Debye–Scherrer rings, were assigned to the *hkl* parameters derived from a hexagonal pattern (100, 110, 200, 210, 300, 220, 310, 400 and 320) as $a = 2.09$ nm (Fig. 9a and S81†).[25] The intense peak at 0.34 nm was assigned to 001 as the stacking distance of **1au**$^+$ in the hexagonal columnar (Col_h) structure ($Z = 1$ for $\rho = 1.79$ g cm^{-3}) (Fig. 9b). Interestingly, heating the powder sample of **2au**$^+$-FABA$^-$ [26] at 190 °C (labelled as **1au**$^+$-FABA^-_H) also formed a Col_h structure identical to that of **1au**$^+$-FABA^-_P (Fig. S79–S82†). In contrast to the tilted **1au**$^+$ plane along the *a*-axis in the single crystal of **1au**$^+$-FABA$^-$, the **1au**$^+$ plane in **1au**$^+$-FABA^-_P should be arranged perpendicularly to the stacking axis, as indicated by the intracolumnar stacking period of 0.34 nm. On the basis of the Col_h structure with $a =$ 2.09 nm and the sizes of **1au**$^+$ and FABA$^-$, columnar structures comprising less-ordered stacking of **1au**$^+$, as indicated by cyan circles, are located close to FABA$^-$, as indicated by magenta circles (Fig. 9b(ii)).

The proximal location of **1au**$^+$ and FABA$^-$ is also suggested by the optimized structure of dimeric **1au**$^+$-FABA$^-$ using B3LYP-GD3BJ/6-31+G(d,p) with LanL2DZ for Au (Fig. 9c). FABA$^-$ should be paired with several **1au**$^+$ in the proximal location, although the XRD pattern suggests that the location of FABA$^-$ is less clear, probably indicating an amorphous-like state. In light of the stoichiometry of the constituents and their contrasting planar and bulky shapes, FABA$^-$ would be observed in three sites on average among the **1au**$^+$ columns, and, in another cross section according to the **1au**$^+$ planes, the anions should be located in the other three sites. As a result, FABA$^-$ can be hexagonally arranged around the **1au**$^+$ columns. The Col_h structure suggested by the XRD pattern is clearly demonstrated by all-atom molecular dynamics (MD) simulations at 25 °C after 100 ns of the equilibration run (Fig. 9d and S66†). Notably, as the initial structure for the MD simulation, the columns comprising tilted **1au**$^+$ units, as observed in the single-crystal structure, are transformed to a structure with barely tilted **1au**$^+$. The combination of planar **1au**$^+$, suitable for stacking, and bulky FABA$^-$, with a less-ordered arrangement *via* noncovalent interactions induces the LeC state.[27,28] The less-ordered FABA$^-$

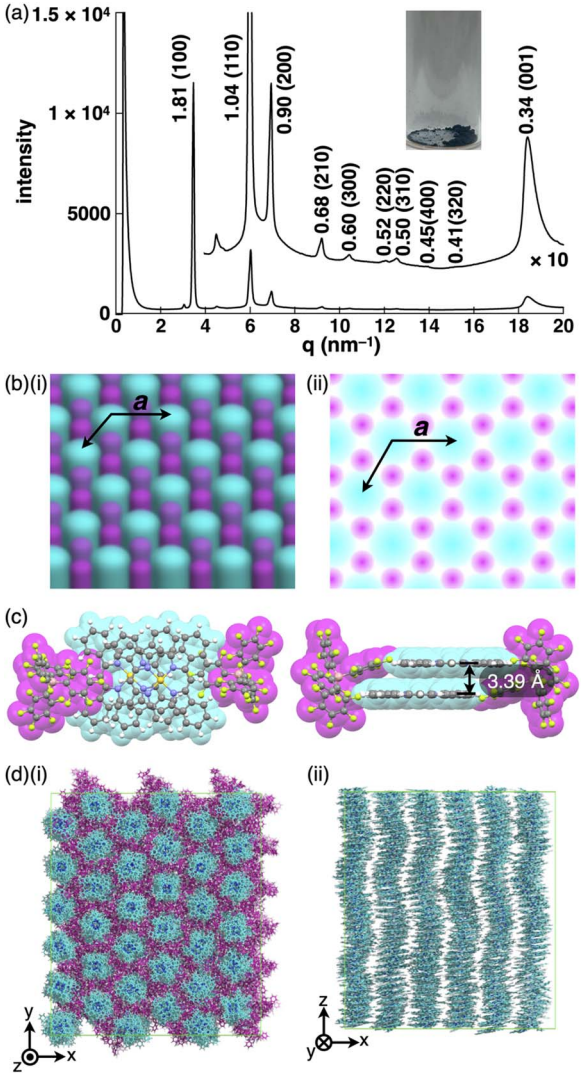

Fig. 9 (a) Synchrotron XRD pattern of **1au**$^+$-FABA^-_P at 25 °C for the sample obtained by precipitation from acetone/*n*-hexane (inset: photograph of the precipitates), (b) schematic representation for the Col_h packing structure: (i) packing diagram and (ii) top view of Col_h (**1au**$^+$ and FABA$^-$ are represented in cyan and magenta, respectively), (c) top and side views of the optimized structure of **1au**$^+$-FABA$^-$ as a dimer using B3LYP-GD3BJ/6-31+G(d,p) with LanL2DZ for Au and (d) snapshot of the MD simulation result for **1au**$^+$-FABA^-_P after 100 ns of the equilibration run at 25 °C showing (i) the top view of the packing diagram and (ii) the side view of **1au**$^+$ columns extracted from the packing diagram (**1au**$^+$ and FABA$^-$ are represented in cyan and magenta, respectively). In (b) (ii), magenta circles suggest the possible locations of FABA$^-$ with a 50% occupancy rate on average in a cross section, whereas cyan circles show the diameter of **1au**$^+$ columns in slipped stacking.

interferes with the ordered packing of **1au**$^+$ for crystallization. **1au**$^+$-FABA^-_P maintains the Col_h structure up to 195 °C and is converted to a complicated crystalline state at higher temperatures, with decomposition at 355 °C. This behaviour is also supported by differential scanning calorimetry (DSC) analysis (Fig. S78†). The appearance of **1au**$^+$-FABA^-_P as a dark blue powder in polarized optical microscopy (POM) was maintained through the heating process. The condition-dependent

assembly (single-crystal and LeC states) as pseudo-polymorphism[29] is fascinating for tuneable properties according to the arrangement of building blocks. The Col_h LeC state, in the absence of aliphatic chains, is rare[28] but can be achieved by pairing the planar π-electronic cation with a bulky counteranion.[30]

The details of the structures of **1au**$^+$-FABA$^-$ were investigated by solid-state NMR (SSNMR) spectroscopy. ^{13}C NMR was performed using cross-polarization magic-angle spinning (CPMAS) (Fig. 10 and S86†). Dipolar dephasing experiments were conducted to support the signal assignment for the ion pair (Fig. S86 and S88†). The broad signals at 132.2, 120.8, 93.4 and 89.3 ppm were assigned to **1au**$^+$, whereas those at 149.7, 137.7 and 126.0 ppm were assigned to FABA$^-$ (Fig. 10a). ^{13}C CPMAS NMR of **1au**$^+$-FABA^-_H showed slightly broader signals than **1au**$^+$-FABA^-_P, suggesting the formation of a more disordered arrangement of constituting ions (Fig. 10b). In contrast, ^{13}C CPMAS NMR for **1au**$^+$-FABA$^-$ as single crystals showed narrower signals than those of **1au**$^+$-FABA^-_P and **1au**$^+$-FABA^-_H (Fig. 10c), suggesting that the broader signals of **1au**$^+$-FABA^-_P and **1au**$^+$-FABA^-_H indicated a less-ordered arrangement of ions that form Col_h structures. Similar signal broadening was observed for ^{19}F and ^{11}B MAS NMR of **1au**$^+$-FABA^-_P and **1au**$^+$-FABA^-_H (Fig. S89 and S90†). Moreover, the characteristic up-field split signals at 93.4 and 89.3 ppm in **1au**$^+$-FABA^-_P are derived from unsubstituted *meso*-carbons,[31] as also suggested by theoretically estimated NMR signals for **1au**$^+$ using B3LYP/6-311+G(d,p) with SDD for Au (Fig. S65†).[12] Such signal splitting is also observed in the ^{13}C CPMAS NMR of the single crystals due to slipped stacking of **1au**$^+$ observed in the crystal structure of **1au**$^+$-FABA$^-$ (Fig. 5a(i)).[32] These observations, along with the XRD analysis and MD simulation, support a less-ordered slipped stacking structure for **1au**$^+$ in a column of Col_h LeC states, wherein the **1au**$^+$ planes are more perpendicularly arranged to the column compared to those in the single crystal.[33]

The formation of such an LeC state was also observed in the precipitate of **1au**$^+$-BArF^-_P prepared from acetone/*n*-hexane.[34] Similar to **1au**$^+$-FABA^-_P, **1au**$^+$-BArF^-_P shows a Col_h LeC state (a = 2.28 nm, c = 0.34 nm, and Z = 1 for ρ = 1.71 g cm^{-3}) (Fig. S84 and S85†), also exhibiting condition-dependent pseudo-polymorphs. Col_h LeC states in the precipitates were observed for **1au**$^+$-FABA$^-$ and **1au**$^+$-BArF$^-$, which formed orthorhombic and monoclinic single-crystal packing structures, respectively. Such pseudo-polymorphic phenomena are fascinating because stacking of **1au**$^+$ can be easily controlled by the assembly conditions. The electric conductivity ($\phi\Sigma\mu$) values of LeC-state **1au**$^+$-FABA^-_P, **1au**$^+$-FABA^-_H and **1au**$^+$-BArF^-_P were estimated to be 1.2 × 10^{-9}, 1.0 × 10^{-9} and 3.4 × 10^{-9} m^2 V^{-1} s^{-1}, respectively, suggesting that electrically conductive pathways also exist in the columnar structures of LeC materials, although the values are smaller than those of the corresponding single crystals (Fig. S93†).

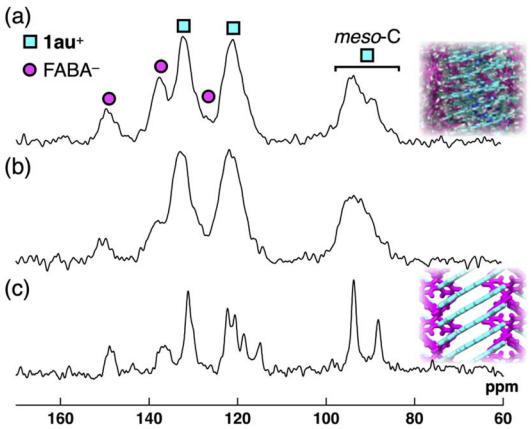

Fig. 10 Solid-state ^{13}C CPMAS NMR spectra of (a) **1au**$^+$-FABA^-_P, (b) **1au**$^+$-FABA^-_H and (c) **1au**$^+$-FABA$^-$ as single crystals recorded at 20 kHz MAS spinning frequency at r.t. with the corresponding packing diagrams.

Conclusions

Ion-pairing assemblies in charge-segregated modes were constructed from a highly planar expanded π-electronic cation in combination with counteranions. Charge-segregated assemblies were formed with both planar and bulky counteranions by means of stable stacked structures of the expanded π-electronic cation. The stacking arrangement and resulting absorption spectra in the single crystals were modulated by coexisting anions. Depending on crystallizing solvent conditions, ion pairs with bulky borate anions also provided LeC states as pseudo-polymorphs of their single crystals. Both single crystals and LeC states exhibited electric conductive properties due to stacking of the π-expanded porphyrin Au^{III} complex.[35] It is noteworthy that the discussed planar π-electronic cation, benzoporphyrin Au^{III} complex, is soluble in organic solvents in the ion-pairing states. Ion pairing is an effective strategy to increase the solubility of planar π-electronic systems for their facile handling and the fabrication of assembled structures with ordered arrangements. Further modifications of charged π-electronic systems would lead to ion-pairing assemblies that can be applied for functional electronic materials and devices.

Data availability

Data supporting the work in this publication are available *via* the ESI and associated crystallographic data.

Author contributions

H. M. designed and conducted the project. Y. H., R. N., Y. M. and H. T. carried out the synthesis, characterization and property examinations. W. C. and S. Se. evaluated the electric conductivities. S. Sa., H. B., Y. I. and G. W. conducted the MD calculations. K. B. and K. T. conducted the transfer integral calculations. K. D., S. O., K. H. and T. N. evaluated the SSNMR. Y. I. and T. A. recorded the solid-state absorption spectra. K. O. supported the discussion on the assemblies.

Conflicts of interest

There are no conflicts of interest to declare.

Acknowledgements

This work was supported by JSPS KAKENHI Grant Numbers JP18H01968, JP22H02067 and JP23K23335 for Scientific Research (B), JP19K05444 and JP24K08389 for Scientific Research (C), JP20J22745 for JSPS Fellows, JP23K17951 for Challenging Research (Exploratory) and JP20H05863 for Transformative Research Areas (A) "Condensed Conjugation", JST SPRING, Grant Number JPMJSP2101 and Ritsumeikan Global Innovation Research Organization (R-GIRO) project (2017–22 and 2022–27). Theoretical calculations were partially performed using the Research Center for Computational Science, Okazaki, Japan (Projects: 20-IMS-C079, 21-IMS-C077, 22-IMS-C077, 23-IMS-C069 and 24-IMS-C067). Synchrotron-radiation analysis was performed at BL40XU (2021B1703 and 2022B1149), BL02B1 (2024A1644) and BL40B2 (2021B1828, 2022A1689, 2022B1546, 2023A1331, 2023B1409 and 2024A1463) of SPring-8 with the approval of the Japan Synchrotron Radiation Research Institute (JASRI). A part of this work was supported by "Advanced Research Infrastructure for Materials and Nanotechnology in Japan (ARIM)" of the Ministry of Education, Culture, Sports, Science and Technology (MEXT). We thank Dr Noboru Ohta, JASRI/SPring-8, for synchrotron-XRD measurements, Dr Nobuhiro Yasuda, JASRI/SPring-8 and Prof. Takuji Hatakeyama, Kyoto University, for single-crystal synchrotron-X-ray analysis, Prof. Osamu Tsutsumi, Ritsumeikan University, for single-crystal X-ray analysis, Prof. Yasuteru Shigeta, University of Tsukuba, for theoretical study and Prof. Hitoshi Tamiaki, Ritsumeikan University, for various measurements.

Notes and references

1 Selected books and reviews on supramolecular assemblies for electronic materials: (*a*) *Functional Supramolecular Architectures: For Organic Electronics and Nanotechnology*, ed. P. Samorì and F. Cacialli, Wiley, Weinheim, 2011; (*b*) *Supramolecular Materials for Opto-Electronics*, ed. N. Koch, RSC, Cambridge, 2015; (*c*) T. Wöhrle, I. Wurzbach, J. Kirres, A. Kostidou, N. Kapernaum, J. Litterscheidt, J. C. Haenle, P. Staffeld, A. Baro, F. Giesselmann and S. Laschat, *Chem. Rev.*, 2016, **116**, 1139–1241; (*d*) J. Urieta-Mora, I. García-Benito, A. Molina-Ontoria and N. Martín, *Chem. Soc. Rev.*, 2018, **47**, 8541–8571; (*e*) P. Yu, Y. Zhen, H. Dong and W. Hu, *Chem*, 2019, **5**, 2814–2853; (*f*) C. J. Kousseff, R. Halaksa, Z. S. Parr and C. B. Nielsen, *Chem. Rev.*, 2022, **122**, 4397–4419; (*g*) J. Chen, W. Zhang, L. Wang and G. Yu, *Adv. Mater.*, 2023, **35**, 2210772.

2 Y. Haketa, K. Yamasumi and H. Maeda, *Chem. Soc. Rev.*, 2023, **52**, 7170–7196.

3 (*a*) K. Yamasumi, K. Ueda, Y. Haketa, Y. Hattori, M. Suda, S. Seki, H. Sakai, T. Hasobe, R. Ikemura, Y. Imai, Y. Ishibashi, T. Asahi, K. Nakamura and H. Maeda, *Angew. Chem., Int. Ed.*, 2023, **62**, e202216013; (*b*) S. Takahashi, M. Murai, Y. Hattori, S. Seki, T. Yanai and S. Yamaguchi, *J. Am. Chem. Soc.*, 2024, **146**, 22642–22649; (*c*) K. Yamasumi, H. Horita, Y. Haketa, S. Seki, K. Bulgarevich, K. Takimiya, H. Shimogawa and H. Maeda, *Chem.–Eur. J.*, 2025, **31**, e202404781.

4 Selected reports of porphyrin Au^{III} complexes: (*a*) E. B. Fleischer and A. Laszlo, *Inorg. Nucl. Chem. Lett.*, 1969, **5**, 373–376; (*b*) R. Timkovich and A. Tulinsky, *Inorg. Chem.*, 1977, **16**, 962–963; (*c*) M. E. Jamin and R. T. Iwamoto, *Inorg. Chim. Acta*, 1978, **27**, 135–143.

5 (*a*) Y. Haketa, Y. Bando, Y. Sasano, H. Tanaka, N. Yasuda, I. Hisaki and H. Maeda, *iScience*, 2019, **14**, 241–256; (*b*) H. Tanaka, Y. Kobayashi, K. Furukawa, Y. Okayasu, S. Akine, N. Yasuda and H. Maeda, *J. Am. Chem. Soc.*, 2022, **144**, 21710–21718; (*c*) Y. Maruyama, K. Harano, H. Kanai, Y. Ishida, H. Tanaka, S. Sugiura and H. Maeda, *Angew. Chem., Int. Ed.*, 2025, **64**, e202415135.

6 A review and selected reports of benzoporphyrins: (*a*) C. M. B. Carvalho, T. J. Brocksom and K. T. de Oliveira, *Chem. Soc. Rev.*, 2013, **42**, 3302–3317; (*b*) R. P. Linstead and F. T. Weiss, *J. Chem. Soc.*, 1950, 2975–2981; (*c*) C. O. Bender, R. Bonnett and R. G. Smith, *J. Chem. Soc. C*, 1970, 1251–1257; (*d*) C. O. Bender, R. Bonnett and R. G. Smith, *J. Chem. Soc., Perkin Trans. 1*, 1972, **6**, 771–776; (*e*) M. G. H. Vicente, A. C. Tomé, A. Walter and A. S. Cavaleiro, *Tetrahedron Lett.*, 1997, **38**, 3639–3642; (*f*) S. Ito, T. Murashima, N. Ono and H. Uno, *Chem. Commun.*, 1998, 1661–1662; (*g*) P. B. Shea, J. Kanicki, L. R. Pattison, P. Petroff, M. Kawano, H. Yamada and N. Ono, *J. Appl. Phys.*, 2006, **100**, 034502; (*h*) N. Noguchi, S. Junwei, H. Asatani and M. Matsuoka, *Cryst. Growth Des.*, 2010, **10**, 1848–1853; (*i*) K. Takahashi, B. Shan, X. Xu, S. Yang, T. Koganezawa, D. Kuzuhara, N. Aratani, M. Suzuki, Q. Miao and H. Yamada, *ACS Appl. Mater. Interfaces*, 2017, **9**, 8211–8218.

7 (*a*) O. W. Webster, *J. Am. Chem. Soc.*, 1965, **87**, 1820–1821; (*b*) T. Sakai, S. Seo, J. Matsuoka and Y. Mori, *J. Org. Chem.*, 2013, **78**, 10978–10985.

8 $\mathbf{2au}^+$ can be obtained as a single isomer prepared from the separated isomer of **2**. Details on the synthetic procedures and properties will be discussed elsewhere.

9 P. R. Spackman, M. J. Turner, J. J. McKinnon, S. K. Wolff, D. J. Grimwood, D. Jayatilaka and M. A. Spackman, *J. Appl. Crystallogr.*, 2021, **54**, 1006–1011.

10 W. Lu, K. T. Chan, S.-X. Xu, Y. Chen and C.-M. Che, *Chem. Sci.*, 2012, **3**, 752–755.

11 The dimerization constant (K_{dim}) for $\mathbf{2au}^+$-$FABA^-$ was estimated to be 1.1×10^5 M^{-1} from the monomer/dimer ratio of ^1H NMR signals in CD_2Cl_2 (5×10^{-5} M) at 20 °C (Fig. S73†).

12 M. J. Frisch, G. W. Trucks, H. B. Schlegel, G. E. Scuseria, M. A. Robb, J. R. Cheeseman, G. Scalmani, V. Barone, G. A. Petersson, H. Nakatsuji, X. Li, M. Caricato, A. V. Marenich, J. Bloino, B. G. Janesko, R. Gomperts, B. Mennucci, H. P. Hratchian, J. V. Ortiz, A. F. Izmaylov, J. L. Sonnenberg, D. Williams-Young, F. Ding, F. Lipparini, F. Egidi, J. Goings, B. Peng, A. Petrone, T. Henderson, D. Ranasinghe, V. G. Zakrzewski, J. Gao, N. Rega, G. Zheng, W. Liang, M. Hada, M. Ehara, K. Toyota, R. Fukuda, J. Hasegawa, M. Ishida, T. Nakajima, Y. Honda,

O. Kitao, H. Nakai, T. Vreven, K. Throssell, J. A. Montgomery Jr, J. E. Peralta, F. Ogliaro, M. J. Bearpark, J. J. Heyd, E. N. Brothers, K. N. Kudin, V. N. Staroverov, T. A. Keith, R. Kobayashi, J. Normand, K. Raghavachari, A. P. Rendell, J. C. Burant, S. S. Iyengar, J. Tomasi, M. Cossi, J. M. Millam, M. Klene, C. Adamo, R. Cammi, J. W. Ochterski, R. L. Martin, K. Morokuma, O. Farkas, J. B. Foresman and D. J. Fox, *Gaussian 16, Revision C.01*, Gaussian, Inc., Wallingford CT, 2016.

13 **1au**$^+$ with $BArF^-$ was also soluble in CH_2Cl_2 and MeOH, whereas the PF_6^- ion pair showed less solubility in the solvents that were available for **1au**$^+$-FABA$^-$.

14 K_{dim} of **1au**$^+$ for **1au**$^+$-FABA$^-$ in DMSO-d_6 was estimated to be 400 M^{-1}.

15 Single crystals of **1au**$^+$-FABA$^-$ prepared from acetone/1,2-dichloroethane also afforded a similar packing structure.

16 Articles for GAMESS: (*a*) M. W. Schmidt, K. K. Baldridge, J. A. Boatz, S. T. Elbert, M. S. Gordon, J. H. Jensen, S. Koseki, N. Matsunaga, K. A. Nguyen, S. Su, T. L. Windus, M. Dupuis and J. A. Montgomery Jr, *J. Comput. Chem.*, 1993, **14**, 1347–1363; (*b*) M. S. Gordon and M. W. Schmidt, In *Theory and Applications of Computational Chemistry: The First Forty Years* ed. C. E. Dykstra, G. Frenking, K. S. Kim and G. E. Scuseria, Elsevier, 2005.

17 M. J. S. Phipps, T. Fox, C. S. Tautermann and C.-K. Skylaris, *Chem. Soc. Rev.*, 2015, **44**, 3177–3211.

18 Report for FMO: K. Kitaura, E. Ikeo, T. Asada, T. Nakano and M. Uebayasi, *Chem. Phys. Lett.*, 1999, **313**, 701–706.

19 Report for pair interaction energy decomposition analysis (PIEDA): D. G. Fedorov and K. Kitaura, *J. Comput. Chem.*, 2007, **28**, 222–237.

20 (*a*) A. Acharya, S. Seki, A. Saeki, Y. Koizumi and S. Tagawa, *Chem. Phys. Lett.*, 2005, **404**, 356–360; (*b*) S. Seki, A. Saeki, T. Sakurai and D. Sakamaki, *Phys. Chem. Chem. Phys.*, 2014, **16**, 11093–11113.

21 Program and report for calculation of transfer integrals: (*a*) ADF (2024.1), SCM, *Theoretical Chemistry*, Vrije Universiteit, Amsterdam, 2024; (*b*) G. te Velde, F. M. Bickelhaupt, E. J. Baerends, C. Fonseca Guerra, S. J. A. van Gisbergen, J. G. Snijders and T. Ziegler, *J. Comput. Chem.*, 2001, **22**, 931–967.

22 T. Mori, A. Kobayashi, Y. Sasaki, H. Kobayashi, G. Saito and H. Inokuchi, *Bull. Chem. Soc. Jpn.*, 1984, **57**, 627–633.

23 Hole transport can be acceptable in light of the electronic properties of **1au**$^+$. Theoretical studies revealed a higher HOMO of **1au**$^+$ than that of **2au**$^+$, suggesting that π-expanded **1au**$^+$, which is positively charged, would be suitable for hole transport (Fig. S35 and S40†). In addition, the HOMO of **1au**$^+$ is comparable to those of typical hole-transporting materials (ref. 1*d*).

24 Other precipitation conditions such as rapid precipitation using $CH_3CN/CHCl_3$ afforded crystalline precipitates with a packing structure similar to the single-crystal structure (Fig. S83†).

25 Small diffraction peaks would be derived from the unidentified packing structure of a minor species formed in the precipitation process.

26 The powder sample of **2au**$^+$-FABA$^-$ was prepared by precipitating from CH_2Cl_2/*n*-hexane.

27 K. Ohta, *Physics and Chemistry of Molecular Assemblies*, World Scientific, 2020.

28 Selected examples of liquid crystals and plastic crystals based on π-electronic molecules that have no aliphatic chains: (*a*) S. Basurto, S. García, A. G. Neo, T. Torroba, C. F. Marcos, D. Miguel, J. Barberá, M. B. Ros and M. R. de la Fuente, *Chem.–Eur. J.*, 2005, **11**, 5362–5376; (*b*) D. Pucci, I. Aiello, A. Aprea, A. Bellusci, A. Crispini and M. Ghedini, *Chem. Commun.*, 2009, 1550–1552; (*c*) Y. Takagi, K. Ohta, S. Shimosugi, T. Fujii and E. Itoh, *J. Mater. Chem.*, 2012, **22**, 14418–14425; (*d*) H. Nakamura, K. Sugiyama, K. Ohta and M. Yasutake, *J. Mater. Chem. C*, 2017, **5**, 7297–7306; (*e*) K. Goossens, L. Rakers, B. Heinrich, G. Ahumada, T. Ichikawa, B. Donnio, T. J. Shin, C. W. Bielawski and F. Glorius, *Chem. Mater.*, 2019, **31**, 9593–9603; (*f*) P. Guragain, M. Powers, J. Portman, B. Ellman and R. J. Twieg, *Mater. Adv.*, 2023, **4**, 4129–4137.

29 B. Dario and G. Fabrizia, *Chem. Soc. Rev.*, 2000, **29**, 229–238.

30 The LeC states in this study might be considered as liquid crystals. The details will be discussed elsewhere.

31 M. Okazaki and C. A. McDowell, *J. Am. Chem. Soc.*, 1984, **106**, 3185–3190.

32 A. P. M. Kentgens, B. A. Markies, J. F. van der Pol and R. J. M. Nolte, *J. Am. Chem. Soc.*, 1990, **112**, 8800–8806.

33 Although the current evaluations for the bulk states suggest frozen-state properties at r.t. that are similar to those of single crystals, investigations according to thermal conditions would reveal more detailed information on dynamic thermal motion and less-ordered states.

34 Higher crystallinity compared to **1au**$^+$-FABA$^-{}_P$ was suggested by the XRD analysis.

35 Ion-pairing assemblies in this study, exhibiting unconventional properties derived from charged π-electronic systems, are completely dissimilar from charge-transfer (CT) complexes that are obtained from electronically neutral donor and acceptor molecules. A review of CT complexes: M. Baharfar, A. C. Hillier and G. Mao, *Adv. Mater.*, 2024, **36**, 2406083.